APPLICATION OF LAND SURFACE TEMPERATURE DERIVED FROM ASTER TIR TO IDENTIFY VOLCANIC GAS EMISSION AROUND BANDUNG BASIN

Zaki Hilman[1]*, Asep Saepuloh[2], and Very Susanto[2]

[1] Master Program of Geological Engineering, Bandung Institute of Technology (ITB), Jl. Ganesha No. 10, Bandung, West Java, Indonesia. 40132

[2] Faculty of Earth Sciences and Technology, Bandung Institute of Technology (ITB), Jl. Ganesha No. 10, Bandung, West Java, Indonesia. 40132

*e-mail: zakihilman1011@gmail.com

Abstract. Gas emission in volcanic areas is one of the features that can be used for geothermal exploration and to monitor volcanic activity. Volcanic gases are usually emitted in permeable zones in geothermal fields. The use of thermal infrared radiometers (TIR) onboard of advanced spaceborne thermal emission and reflection radiometers (ASTER) aims to detect thermal anomalies at the ground surface related to gas emissions from permeable zones. The study area is located around Bandung Basin, West Java (Indonesia), particularly the Papandayan and Domas craters. This area was chosen because of the easily detected land surface temperature (LST) following emissivity and vegetation corrections (T_{cveg}). The ASTER TIR images used in this study were acquired by direct night and day observation, including observations made using visible to near-infrared radiometers (VNIR). Field measurements of volcanic gases composed of SO_2 and CO_2 were performed at three different zones for each of the craters. The measured SO_2 concentration was found to be constant over time, but CO_2 concentration showed some variation in the craters. We obtained results suggesting that SO_2 gas measurements and T_{cveg} are highly correlated. At Papandayan crater, the SO_2 gas concentration was 334.34 ppm and the T_{cveg} temperature was 35.67 °C, results that are considered highly anomalous. The same correlation was also found at Domas crater, which showed an increased SO_2 gas concentration of 35.39 ppm located at a high-anomaly T_{cveg} of 30.65 °C. Therefore, the ASTER TIR images have potential to identify volcanic gases as related to high T_{cveg}.

Keywords: *remote sensing, volcanic gas emission, land surface temperature (LST)*

1 INTRODUCTION

Indonesia is one of the countries with the greatest geothermal energy potential, with a total estimated energy of 29,227 MWe (Saepuloh et al., 2018). Geothermal energy is related to volcanic systems, which at the same time serve as hazards which need to be mitigated. Through the detection of permeable zones, we can observe volcano activities both for mitigation and for geothermal exploration. A permeable zone as a path for hydrothermal fluids can be recognized by the presence of SO_2 and CO_2 together with geothermal features (Moeck, 2014).

Volcanic gases from the subsurface are useful for providing information about magma transportation and degassing processes as well identifying the reservoirs of geothermal systems. Permeable zones at the surface tend to show significant anomalies in temperature and gas readings in concordance with magma activities, and provide indicators of the precursors of volcanic eruption (Oppenheimer, Scaillet, & Martin, 2011).

Remote sensing in volcanic areas has the potential to be used to improve our understanding of volcanic processes,

179

to detect precursor activity for volcanic hazards, and to provide key monitoring data during volcanic hazard events.
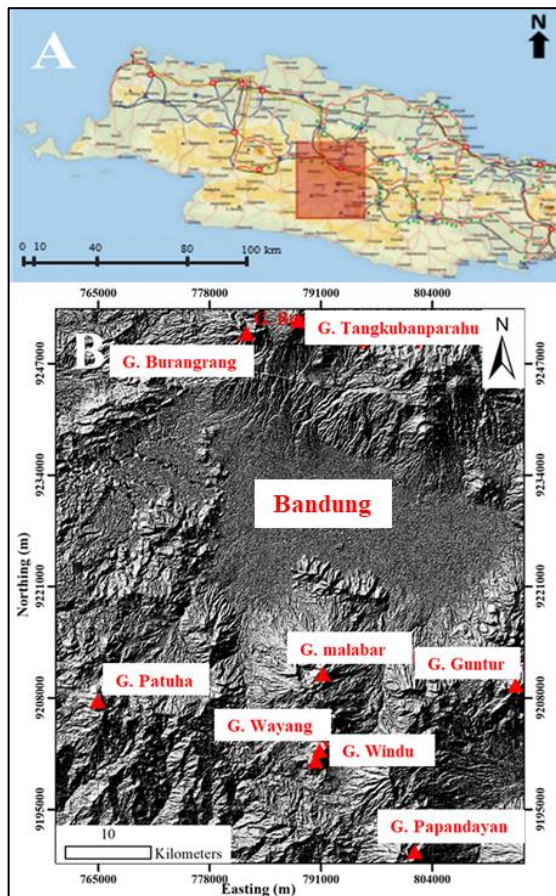

Figure 1-1: Study area in central West Java, Indonesia, represented by the red square in A, and the Bandung Basin including Mt. Papandayan, Mt. Tangkubanparahu and others, depicted by red triangles in B

Satellite instruments have been used successfully to detect passive and explosive degassing volcanic emissions (Hooper, Prata, & Sigmundsson, 2012). The application of thermal remote sensing to the detection of gas emissions as related to surface temperature is crucial for the detection process for surface permeable zone detection. The advanced spaceborne thermal emission and reflection radiometer (ASTER) provides satellite images with the ability to recognize permeable zones based on land surface temperature (LST) (Jimenez-Munoz & Sobrino, 2010). ASTER TIR level 1B data is processed and corrected atmospherically by emissivity and vegetation factors to obtain realistic LST under vegetation cover (Chalik, 2019), and permeable zones associated with geothermal features can be estimated from corrected LST (Nugroho & Domiri 2017). Through this research it is hoped that we can identify volcanic gas emissions from ASTER TIR data.

Bandung is the capital of West Java province, with a population of about 2.5 million people. Because Bandung is surrounded by volcanoes (for example Tangkubanparahu and Galunggung), volcanic activity mitigation is needed to prepare for eruption occurrences (Raharjo, 2017). Bandung is located in the Bandung Basin, and this is one of the reasons it was chosen as the study area. The other reason is that the Bandung Basin has a high variation of surface thermal activities and geothermal features, with Papandayan crater at Mt. Papandayan and Domas crater at Mt. Tangkubanparahu providing field verification and measurements (Figure 1-1).

2   MATERIALS AND METHODOLOGY

In this study, we used five and six ASTER level 1B data for night and day observations, respectively. The ASTER data from night observations were processed to obtain emitted temperature from the TIR. This data was used to calculate LST because of its capability for detecting the physical signature of objects based on their emitted thermal radiation. In addition, the ASTER level 1B data from day observations were processed to obtain reflected signatures from the visible and near-infrared radiometer (VNIR). The ASTER VNIR images were used mainly to compensate for the emissivity and vegetation factor from the TIR images. Level 1B data were selected because of the complete correction applied including radiometric and

geometric parameters from the raw data (Abrams et al., 2002). Therefore, the accuracy of this selected data must be higher than level 1A.

We selected the data acquisition conditions based on the latest acquisition date, and cloud coverage of less than 10%. Details of the acquired data are listed in Table 2-1.

Field measurements of volcanic gases located at Papandayan and Domas craters were used to verify ASTER image analyses. Moreover, characterizing the thermal anomaly detected by ASTER images and measured gases at field level leads to a better understanding of permeable zones as the fluid paths of geothermal systems.

Table 2-1: ASTER images used in this study

No	Granule code	Process-ing level	Acqui-sition date	Acqui-sition time (GMT+7)
1	AST070 62018-28042	Level 1B	2018-07-06	10.18 PM
2	AST070 62018-28037	Level 1B	2018-07-06	10.18 PM
3	AST240 62016-26826	Level 1B	2016-24-06	10.24 PM
4	AST240 62016-26824	Level 1B	2016-24-06	10.24 PM
5	AST240 62016-26820	Level 1B	2016-24-06	10.24 PM
6	AST300 72018-8127	Level 1B	2018-30-07	10.19 AM
7	AST300 72018-8132	Level 1B	2018-30-07	10.19 AM
8	AST300 72018-8138	Level 1B	2018-30-07	10.19 AM
9	AST090 62017-8142	Level 1B	2017-09-06	10.17 AM
10	AST090 72014-8145	Level 1B	2014-19-07	10.18 AM
11	AST090 72014-8675	Level 1B	2014-19-07	10.18 AM

Two main steps were used to obtain the data for gas anomalies related to LST used in this study. First, we extracted LST from the ASTER TIR night observations and corrected using vegetation analyses based on ASTER VNIR for the day observations. Then field measurements including ground temperature and SO_2 and CO_2 gas concentrations were collected to validate the corrected LST results. FLIR Thermocouple and Mini Sensync volcanic gas detectors were used to measure ground temperature and gas concentrations (Hilman, Saepuloh, Chalik, & Heriawan, 2020).

The ASTER TIR images were processed to calculate the brightness temperature (BT) using the temperature emissivity separation method (Jimenez-Munoz & Sobrino, 2010). The BT images indicating the brightness level of the pixels from the thermal images were then corrected by the emissivity and vegetation parameters to obtain the LST for corrected vegetation (T_{cveg}), using the following formula:

$$T_{cveg} = 2T_{em} - T_v \tag{2-1}$$

where T_{cveg} = LST corrected vegetation, T_{em} = LST corrected emissivity and T_v = vegetation temperature.

The spatial resolution of the ASTER TIR image of 90 × 90 m was resampled to 15 × 15 m. A full explanation of the formula used to obtain T_{cveg} can be found in the study by Hilman et al. (2020).

3 RESULTS AND DISCUSSION

The T_{cveg} map showed a range of surface temperature of 13.1 to 47.7 °C (Figure 3-1). The map was used as a basis for field verification and measurements. The NW–SE line on the T_{cveg} image originated from discontinuing acquisition times due to different footprints of the ASTER satellite. Following the extraction of the T_{cveg}, the location for gas

measurement points was determined for validation and field measurements. The high-anomaly T_{cveg} for Papandayan crater of Mt. Papandayan and Domas crater of Mt. Tangkubanparahu were then selected.
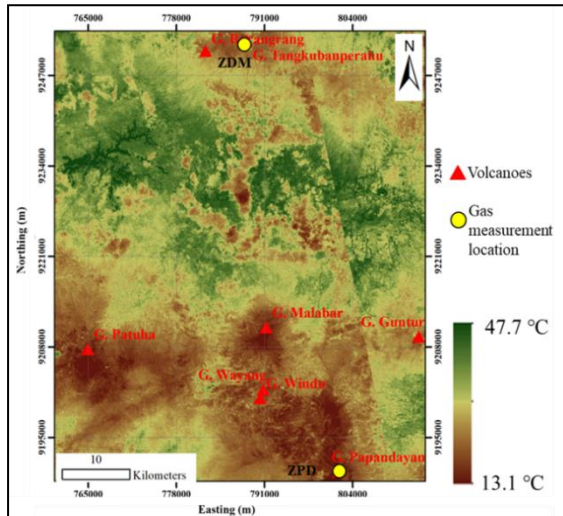

Figure 3-1: LST image corrected by vegetation (T_{cveg}) from ASTER TIR night observation

Gas concentrations were measured at three T_{cveg} high-anomaly zones at Papandayan crater. Figure 3-2 shows the measurement zone, which is located in the middle of the crater. In the case of Domas crater, Figure 3-3 shows that the three T_{cveg} high-anomaly zones that can be measured were located in the southern area of the crater, this is due to limited access to the other area. The gas concentration for each zone was measured over 30 to 80 minutes to observe the variation in gas concentration (Figure 3-4).

The measurement results for SO_2 gas concentration at the Papandayan and Domas craters show a constant level over the measurement time. This phenomenon indicates that there was a constant supply of SO_2 gas from the subsurface. The SO_2 gas concentration at Papandayan crater was 300 to 350 ppm,

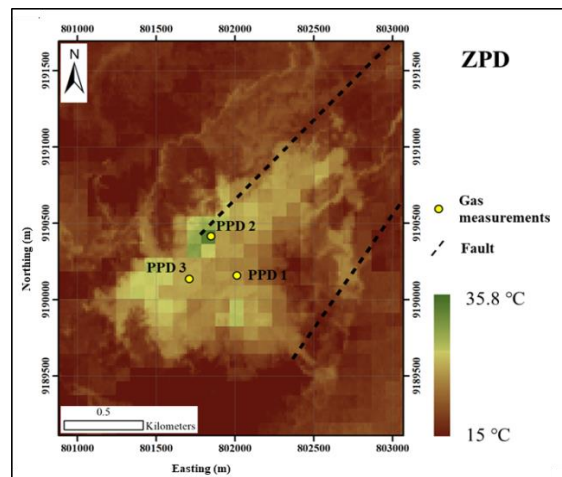higher than at Domas crater, which was between 20 and 40 ppm.

Figure 3-2: SO_2 and CO_2 gas measurement zones at Papandayan crater.

Generally, the CO_2 gas concentration at Papandayan crater showed a decreasing pattern over the measured time. In contrast, the concentration of CO_2 at Domas crater showed an increase over the measured time. Gas concentration could be affected by the amount of organic material buried beneath the surface, which increases readings for CO_2 (Granados & Jenkins, 2015).
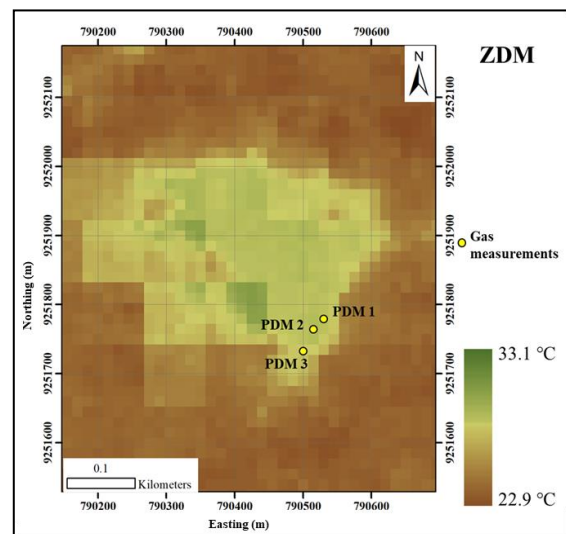

Figure 3-3: SO_2 and CO_2 gas measurement zones at Domas crater

The CO_2 gas concentrations at Papandayan and Domas craters were measured at about 1,000 to 4,000 ppm and 3,000 to 6,000 ppm, respectively.

According to the high-anomaly zones of T_{cveg} and gas concentrations measured in the field, correlation was achieved in particular for SO_2 gas concentrations, as shown in Table 3-5.

The SO_2 gas concentration was strongly in concordance with high T_{cveg}. The highest T_{cveg} was about 35.7°C for Papandayan crater, located at PPD2 with an average SO_2 gas concentration of about 334.3 ppm. Discrepancies were observed at PPD1 and PPD3, with the lowest T_{cveg} of about 26 and 28 °C, respectively being found there. These also had high SO_2 gas concentration, at 320 and 329 ppm, respectively.
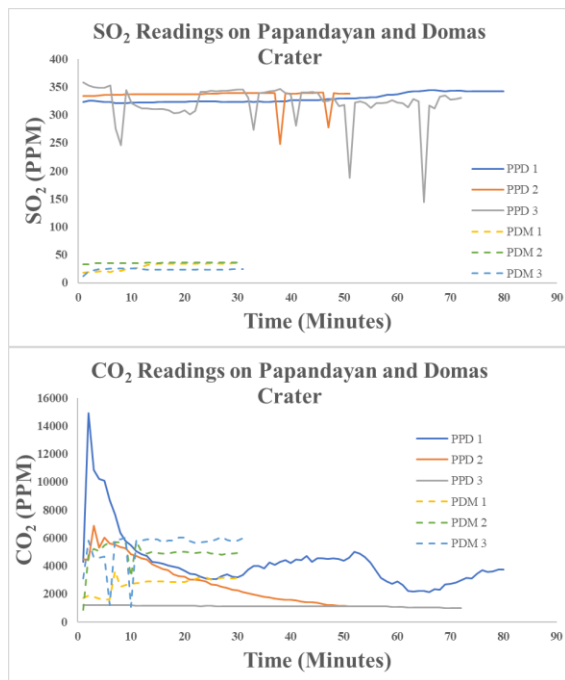

Figure 3-4: The variation of SO_2 and CO_2 gas concentrations at Papandayan and Domas craters.

The high-anomaly T_{cveg} of around 30 °C at the Domas crater showed a good correlation with the highest to the lowest concentrations of SO_2, as measured at PDM2, PDM1 and PDM3 of 35.4, 29.3 and 23.5 ppm, respectively. However, the correlation of CO_2 gas concentration with T_{cveg} was low.

The measured CO_2 gas concentration varied between Papandayan and Domas craters. Papandayan crater was characterized by decreasing CO_2 concentration, but concentration at Domas crater was relatively constant.

Following from the correlation between high-anomaly T_{cveg} and SO_2 gas concentration, we suggest that permeable zones at the surface could be identified by the presence of high gas concentration, as indicated by high-anomaly T_{cveg}. Therefore, identifying high-anomaly T_{cveg} in a volcanic area series will be useful for monitoring volcanic activity resulting from magma ascending to the near surface releasing large amounts of SO_2 gas (Oppenheimer et al., 2011). Based on our results, high concentration of SO_2 gas seems to correlate with high anomalies observed at T_{cveg} locations.

Although high-anomaly T_{cveg} was found both at the Papandayan crater and the Domas crater, the average SO_2 gas concentration at the Domas crater was lower than at the Papandayan crater. We interpreted that the difference in geological framework and geochemical composition of hydrothermal fluids might control the gas that is released to the surface. This result is in agreement with a previous report which confirmed that the gas concentrations for Domas crater were low SO_2 and high CO_2. This report also mentioned that SO_2 gas concentration at Domas crater was relatively low compared with H_2O and CO_2 gas concentrations (Nasution, Kartabinata, Sutamingsih, & Hadisantono, 2004).

Table 3-1: Mean SO_2 and CO_2 readings at Papandayan and Domas craters

Sampling code	T_{cveg} (°C)	Mean SO_2 (PPM)	Mean CO_2 (PPM)
PPD1	26.72	329.42	4257.04
PPD2	35.67	334.34	2976.8
PPD3	27.79	320.95	1117.69
PDM1	30.23	29.27	2707.67
PDM2	30.65	35.39	4894.81
PDM3	29.4	23.46	5334.71

4   CONCLUSIONS

We investigated the effectiveness of LST extraction based on corrected vegetation and emissivity (T_{cveg}) using ASTER TIR night observations. The proposed technique is proven to be useful for identifying the possibility of gas release at permeable zones which is characterized by increased gas concentration at geothermal features.

According to the SO_2 and CO_2 gas concentration measurements, the SO_2 concentration was in concordance with high-anomaly T_{cveg}. The SO_2 gas concentration increased at a higher T_{cveg}, and vice versa, with exceptions in PPD1 and PPD3. The rainy conditions when measuring PPD3 could have caused the measured gas concentration to be lower than PPD1, given its higher T_{cveg} reading. The SO_2 gas concentration level was relatively constant at both Papandayan and Domas craters. The difference CO_2 gas concentration between Papandayan and Domas craters was interpreted as being due to their contrasting vapour- and water-dominated geothermal systems, respectively. Further study is necessary to improve the calculated T_{cveg} for quantifying gas emission or leakage from volcanoes as well as for permeable zones in geothermal systems.

ACKNOWLEDGEMENTS

AUTHOR CONTRIBUTIONS

Application Of Land Surface Temperature Derived From Aster Tir To Identify Volcanic Gas Emission Around Bandung Basin. Lead Author: Zaki Hilman; Co-Author: Asep Saepuloh dan Very Susanto.

REFERENCES

Abrams, M., Hook, S., & Ramachandran, B. (2002). *ASTER Users Handbook* (2nd ed.). Pasadena, California: NASA Jet Propulsion Laboratory

Chalik, C. A. (2019). *Karakteristik Anomali Suhu Permukaan Tanah Berdasarkan Citra ASTER Terkoreksi Vegetasi di Daerah Panasbumi (Studi Kasus Lapangan Panasbumi Patuha) [Characteristics of soil surface temperature anomalies based on ASTER image corrected vegetation in geothermal areas (case study of the Patuha geothermal field)]* (Thesis), Institut Teknologi Bandung, Indonesia.

Granados, H. D., & Jenkins, S. (2015). Extreme volcanic risks 1: Mexico City. In J. F. Schroeder & P. Papale (Eds.), *Volcanic Hazards, Risks, and Disasters* (pp. 315–354). doi: 10.1016/B978-0-12-396453-3.00013-7

Hilman, Z., Saepuloh, A., Chalik, C. A., & Heriawan, M. N. (2020). Identifying upflow zone based on thermal infrared (TIR) sensor and field measurements at volcanic field. *IOP Conference Series: Earth and Environmental Science, 417*, 012011. doi: 10.1088/1755-1315/417/1/012011

Hooper, A., Prata, F., & Sigmundsson, F. (2012). Remote sensing of volcanic hazards and their precursors. *Proceedings of the IEEE, 100*(10), 2908–2930. doi: 10.1109/JPROC.2012.2199269

Jimenez-Munoz, J.-C. & Sobrino, J. (2010). A single-channel algorithm for land-surface temperature retrieval from ASTER data. *Geoscience and Remote Sensing Letters, IEEE 7*, 176–179. doi: 10.1109/LGRS.2009.2029534

Moeck, I. S. (2014). Catalog of geothermal play types based on geologic controls. *Renewable and Sustainable Energy Reviews 37*, 867–882. doi: 10.1016/j.rser.2014.05.032

Nasution, A., Kartabinata, M. N., Sutamingsih, E., & Hadisantono, R. (2004). Geology, age dating and geochemistry of the Tangkuban Parahu Geothermal Area, West Java, Indonesia. *Journal of the Geothermal Research Society of Japan 26*, 285–303. doi: org/10.11367/grsj1979.26.285

Nugroho, U. C. & Domiri, D. D. (2017). Identification of land surface temperature distribution of geothermal area in Ungaran Mount by using Landsat 8 imagery. *International Journal of Remote Sensing and Earth Sciences, 12*(2), 143–150. doi: org/10.30536/j.ijreses.2015.v12.a2708

Oppenheimer, C., , R. (2011). Sulfur degassing from volcanoes: Source conditions, surveillance, plume chemistry, and earth system impacts. *Reviews in Mineralogy and Geochemistry, 73*, 363-421. doi: 10.2138/rmg.2011.73.13

Raharjo, P. P. (2017). Understanding and identifying natural hazard for Bandung City preparedness and mitigation against natural disaster. *MATEC Web Conf. 103*, 07011. doi: 10.1051/matecconf/201710307011

Saepuloh, A., Haeruddin, H., Heriawan, M. N., Kubo, T., Koike, K., & Malik, D. (2018). Application of lineament density extracted from dual orbit of synthetic aperture radar (SAR) images to detecting fluids paths in the Wayang Windu geothermal field (West Java, Indonesia). Geothermics 72, 145–155. doi: 10.1016/j.geothermics.2017.11.010